Electronic Supplementary Material (ESI) for Journal of Materials Chemistry C.

Supplementary Information

In-situ efficient growth of Rubik nanocube $WO_3 \cdot 0.33H_2O$ array films for high-performance electrochromic energy storage device

Sensen Jia, Pengyang Lei, Zhuanpei Wang, Weilong Yang, Jinhui Wang,*

Guofa Cai*

Key Laboratory for Special Functional Materials of Ministry of Education, National & Local Joint Engineering Research Center for High-efficiency Display and Lighting Technology, School of Materials and Engineering, and Collaborative Innovation Center of Nano Functional Materials and Applications, Henan University, Kaifeng 475004, China

*Corresponding author(s). E-mail: jinhui.wang@henu.edu.cn; caiguofa@henu.edu.cn

Proof of the Faraday reaction process

According to the following power law: [1]

$$i = av^b \quad (1)$$

Where *i* is the peak current and *v* is the scan rate, and a and *b* refer to the adjustable parameters.

Calculation of areal specific capacitance (Ca)

The C_a can be calculated at different current densities from the GCD curves according to the following equation: [2]

$$C_a = \frac{2I \int_{t(V_{max})}^{t(V_{min})} V(t)dt}{A(V_{max} - V_{min})^2} \quad (2)$$

Where C_a and *A* represent the areal capacitance and geometrical area of the electrode involved in the reaction in the electrolyte, V_{max} and V_{min} are the maximum and minimum potential during galvanostatic discharge measurements, respectively. *I* is the current density of charge/discharge.

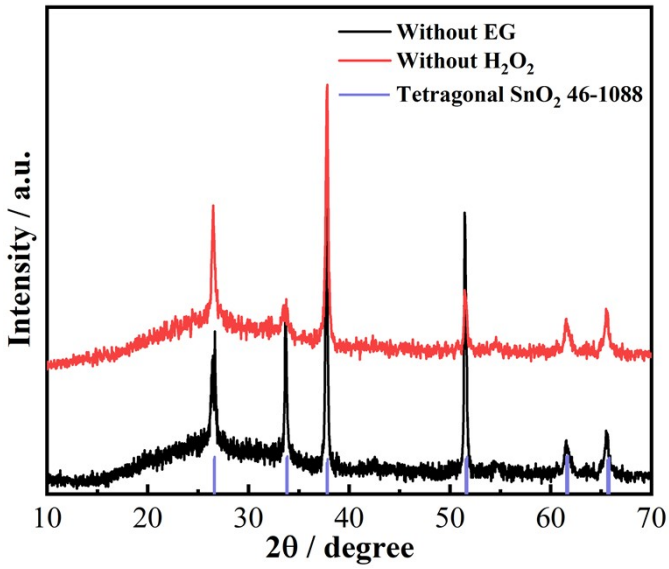

Fig. S1. XRD patterns of the growth of WO_3 film without H_2O_2 and EG on FTO substrates.

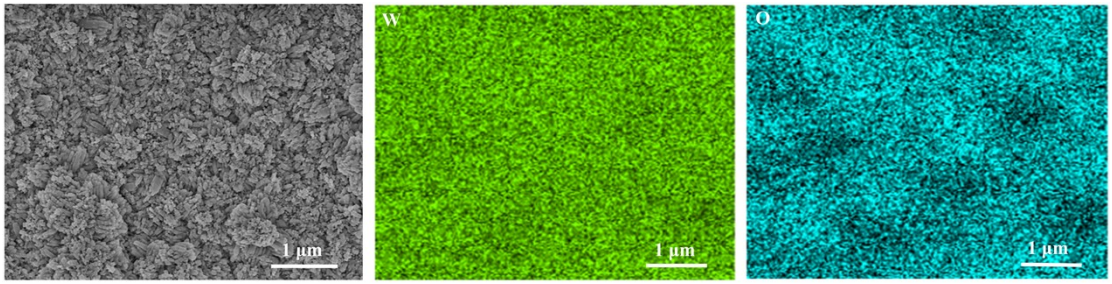

Fig. S2. SEM and EDS mapping images of $WO_3 \cdot 0.33H_2O$ film.

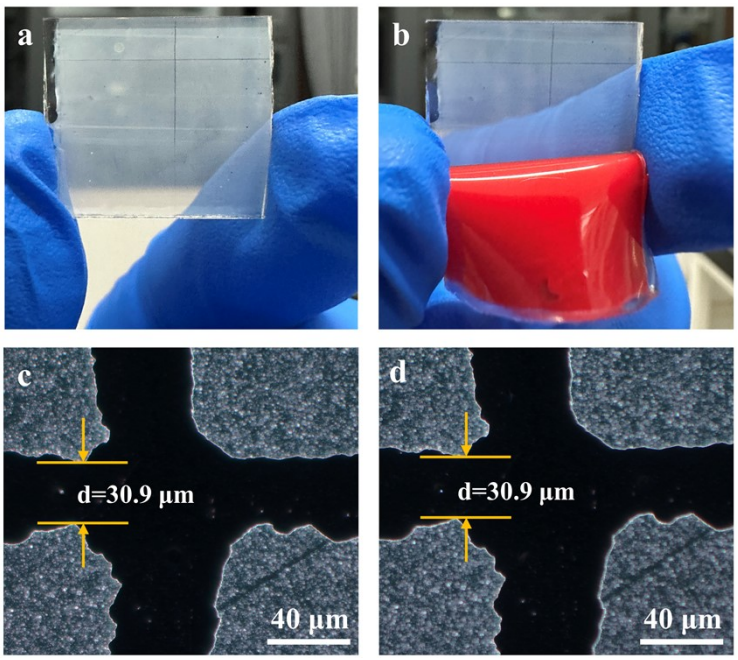

Fig. S3. Digital photographs of the $WO_3 \cdot 0.33H_2O$ films before (a) and after (b) tape adhesion/peeling. Optical microscopes of the $WO_3 \cdot 0.33H_2O$ films before (a) and after (b) tape adhesion/peeling.

The process of tape testing is described as follows: First, the cross structure of the $WO_3 \cdot 0.33H_2O$ film was marked with a knife (bright section in Figure S2a, b). Afterward, commercial tape (3M, 4910-type) was tightly adhered to the surface of the $WO_3 \cdot 0.33H_2O$ film for 5 minutes and then peeled off.

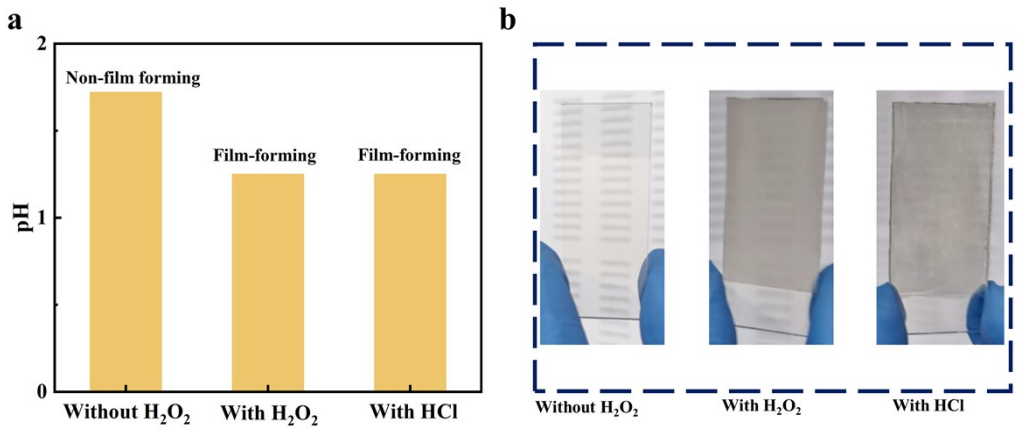

Fig. S4. Comparison of film formation by hydrothermal reaction under different acidic conditions：(a) pH under different acidic conditions. (b) Photo images of film formation in the presence or absence of H_2O_2, and in the presence of HCl, respectively.

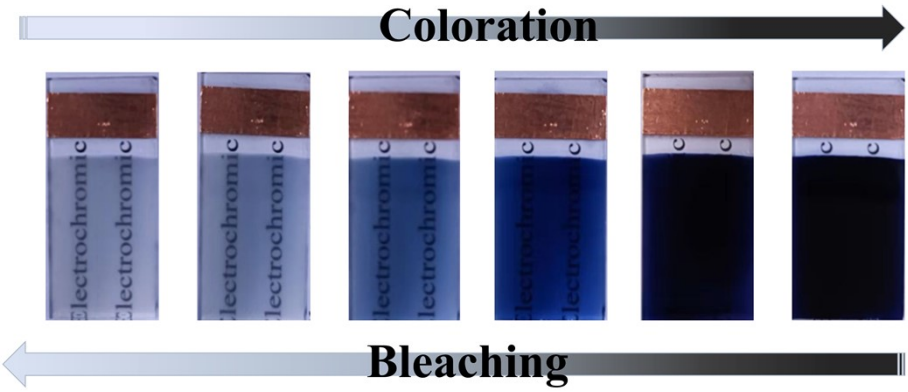

Fig. S5. Image of $WO_3 \cdot 0.33H_2O$ films during the coloring and bleaching process.

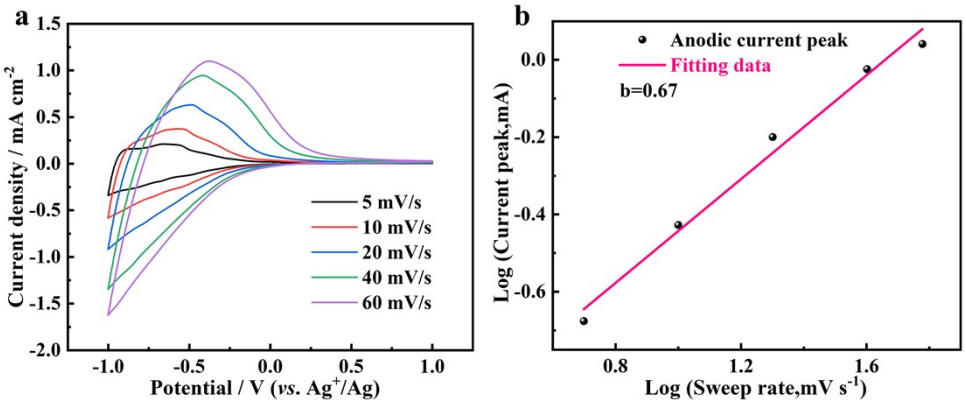

Fig. S6. (a) CV curves of $WO_3 \cdot 0.33H_2O$ film at the potential region of ±1 V at various scan rates ranging from 5 to 60 $mV \cdot s^{-1}$ (b) Calculation of b value from anodic peaks for the electrochromic $WO_3 \cdot 0.33H_2O$ film.

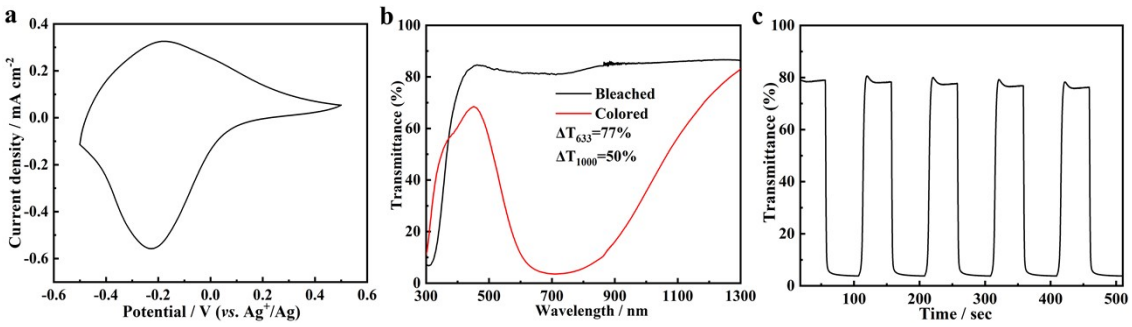

Fig. S7. Electrochromic and electrochemical performance of the PB film in 1 M $LiClO_4$/PC electrolyte. (a) CV curves of the PB film at a scan rate of 20 mV s^{-1} in the potential range from −0.5 to 0.5 V (vs Ag^+/Ag). (b) Optical transmittance spectra of the PB film in the colored (0.5 V vs. Ag^+/Ag, red line) and bleached (-0.5 V vs. Ag^+/Ag, black line) states. (c) In situ transmittance responses of PB film in 633 nm obtained under the applied square-wave potential between -0.5 and 0.5 V for 50 s, respectively.

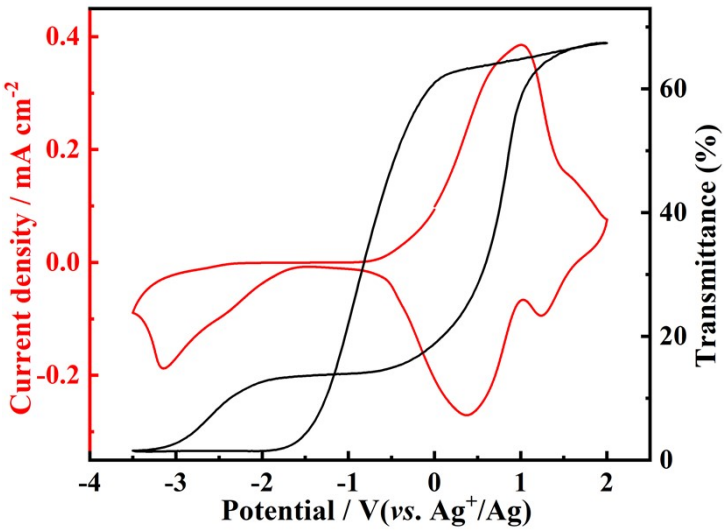

Fig. S8. CV curve and in situ transmittance spectrum of the EESD at 633 nm at a scan rate of 20 mV s^{-1}.

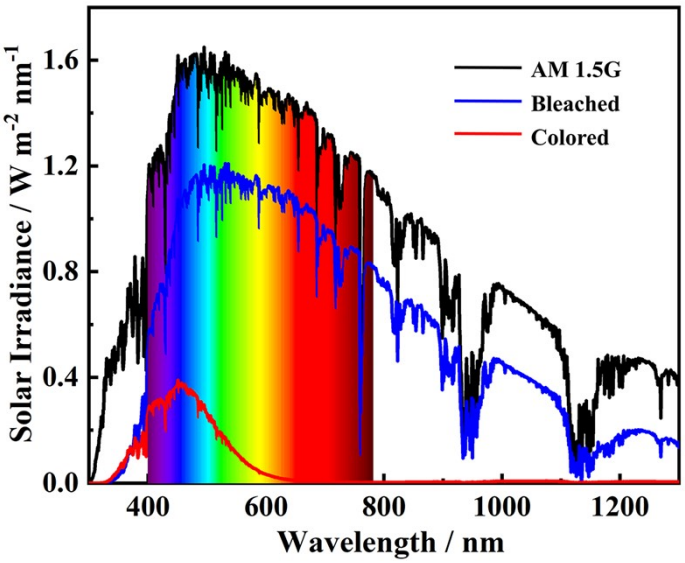

Fig. S9. Solar irradiation spectra of the EESD in bleached and colored states compared to the standard solar radiation curve (AM 1.5G)

Table S1 Electrochromic performance comparisons the thin films obtained with different structural-directing agents.

Sample	ΔT (%)/ λ(nm)	Hydrothermal conditions	CE ($cm^2 \cdot C^{-1}$)	t_b /t_c (s)	Cycle stability (retention)
Hexagonal WO_3[3]	71.5/700	120 ℃，2 h	72.5	10.7/12.4	5000 (90.8%)
Hexagonal WO_3[4]	46/1600	180 ℃，4 h	106.1	3.6/2.4	1000 (96%)
Hexagonal WO_3[5]	66/633	180 ℃，12 h	106.8	3.4/6.7	1000 (-)
Hexagonal WO_3[6]	72.4/550	180 ℃，3 h	67.6	7/3	500 (67%)
Hexagonal WO_3[7]	70.1/680	180 ℃，2.5 h	55.9	3/12	400 (-)
Monoclinic WO_3[8]	32.5/700	180 ℃，2 h	42.37	-	100 (95.5%)
Hexagonal WO_3[9]	64/600	180 ℃，4 h	47	17/10	1000 (96%)
Hexagonal WO_3[10]	33.9/633	180 ℃，24 h	37.6	18/25	-
Orthorhombic WO_3[11]	43/633	180 ℃，2 h	112.7	1.4/4.3	3000 (-)
Hexagonal WO_3[12]	78.1/630	120 ℃，2.5 h	56.5	6/5	15000 (-)
Orthorhombic $WO_3 \cdot 0.33H_2O$	80.6/633	120 ℃, 45 min	65.6	14/15	1000 (80%) (This work)

1. J. W. Torsten Brezesinski, Julien Polleux, Bruce Dunn, Sarah H. Tolbert, J. Am. Chem. Soc., 2009, **131**, 1802-1809.

2. P. Yang, W. Mai, Nano Energy, 2014, **8**, 274-290.

3. Y. Wang, J. Zeng, Z. Zhou, G. Shen, T. Tang, R. U. R. Sagar and X. Qi, Appl. Surf. Sci., 2022, **573**, 151603.

4. L. Wang, Y. Liu, G. Han and H. Zhao, J. Alloy. Compd., 2022, **890**, 161833.

5. M. Dongyun, S. Guoying, W. Hongzhi, Z. Qinghong and L. Yaogang, J. Mater. Chem. A, 2012, **1**, 684.

6. Q. Huang, S. Cao, Y. Liu, Y. Liang, J. Guo, R. Zeng, J. Zhao and B. Zou, Sol. Energy Mat. Sol. C., 2021, **220**, 110853.

7. L. Shen, G. Luo, J. Zheng and C. Xu, Electrochim. Acta, 2018, **278**, 263-270.

8. R. Yu, Z.-h. Meng, M.-d. Ye, Y.-h. Lin, N.-b. Lin, X.-y. Liu, W.-d. Yu and X.-y. Liu, CrystEngComm, 2015, **17**, 6583-6590.

9. F. Zheng, S. Song, F. Lu, R. Li, N. Bu, J. Liu, Y. Li, P. Hu and Q. Zhen, CrystEngComm, 2016, **18**, 3891-3904.

10. E. K. Jinmin Wang, Pooi See Lee,* and Jan Ma, J. Phys. Chem. C, 2009, **113**, 9655–9658.

11. Z. Jiao, X. Wang, J. Wang, L. Ke, H. V. Demir, T. W. Koh and X. W. Sun, Chem. Commun., 2012, **48**, 365-367.

12. J. Pan, Y. Wang, R. Zheng, M. Wang, Z. Wan, C. Jia, X. Weng, J. Xie and L. Deng, J. Mater. Chem. A, 2019, **7**, 13956-13967.